

# Parameter Extraction Approaches for Compact Modeling of Thermoelectric Modules

Hanlong Wan<sup>a1</sup>, Bo Shen<sup>\*a</sup>, Zhenning Li<sup>a</sup>

<sup>a</sup>Oak Ridge National Laboratory, Oak Ridge, TN, USA

\*Corresponding author

[shenb@ornl.gov](mailto:shenb@ornl.gov)

This manuscript has been authored by UT-Battelle, LLC, under contract DE-AC05-00OR22725 with the US Department of Energy (DOE). The US government retains and the publisher, by accepting the article for publication, acknowledges that the US government retains a nonexclusive, paid-up, irrevocable, worldwide license to publish or reproduce the published form of this manuscript, or allow others to do so, for US government purposes. DOE will provide public access to these results of federally sponsored research in accordance with the DOE Public Access Plan (<http://energy.gov/downloads/doe-public-access-plan>).

---

<sup>1</sup> Current address: Pacific Northwest National Laboratory, Richland, WA, USA

## ABSTRACT

Thermoelectric (TE) cooling has experienced rapid advancements with the foundational understanding of TE materials. TE modules, compact and lightweight devices, have become the prevalent approach for implementing TE technologies. Accurately quantifying TE physical parameters (Seebeck coefficient  $\alpha$ , thermal conductivity  $\kappa$ , and thermal resistance  $\rho$ ) is challenging due to the dynamic temperature changes in operation. Furthermore, extracting lumped property parameters is crucial for designing energy systems using TE modules. Existing research has several limitations, such as lack of comparative analysis between prevalent formulae, reliance on potentially inaccurate vendor-supplied data, disregard for fundamental assumptions, and absence of empirical measurements. This study addresses these gaps by conducting TE material characterization, comparing three existing formulae using vendor datasheets, designing a laboratory test facility for model validation and refinement, and outlining a structured data extraction procedure. The study's novelty lies in multiple key contributions: (1) a detailed comparative analysis of existing formulae for extracting TE property parameter; (2) executing experimental work in a laboratory setting to validate the model and elucidate its limitations; (3) highlighting potential risks; (4) clarifying possible assumptions from both material and engineering perspectives; and (5) considering temperature differential impacts. This comprehensive approach addresses the current research gaps and provides valuable insights into the design and application of TE modules in various energy systems.

Keywords: thermoelectric, heat pump, Seebeck coefficient, coefficient of performance, materials

## NOMENCLATURE

$A$	area ( $\text{m}^2$ )
$c_p$	specific heat ( $\text{J}\cdot\text{kg}^{-1}\cdot\text{K}^{-1}$ )
$D$	characteristic linear dimension (m)
$d$	length of side (m)
$DT$	temperature difference (K)
$f$	fill factor
$h$	enthalpy ( $\text{J}\cdot\text{kg}^{-1}$ )
$H$	height (m)
$I$	current (A)
$k$	liquid thermal conductivity ( $\text{W}\cdot\text{m}^{-1}\cdot\text{K}^{-1}$ )
$L$	length (m)
LMTD	Logarithmic Mean Temperature Difference
$l$	thickness (m)
$MFR$	Mass Flow Rate ( $\text{kg}\cdot\text{s}^{-1}$ )
$N$	number
$Nu$	Nusselt number
$Pr$	Prandtl number
$Q$	capacity (J)
$R$	lumped electric resistance ( $\Omega$ )
$Re$	Reynolds number
$RME$	relative mean error
$S$	lumped Seebeck coefficient ( $\text{V}\cdot\text{K}^{-1}$ )
$s$	Seebeck coefficient ( $\text{V}\cdot\text{K}^{-1}$ )
$T$	surface or liquid temperature (K)
TE	thermoelectric
TEHP	thermoelectric heat pump
$U$	voltage (V)
$u$	liquid flow speed ( $\text{m}\cdot\text{s}^{-1}$ )
$UA$	heat transfer coefficient and area ( $\text{W}\cdot\text{K}^{-1}$ )
$x$	length (m)
$Z$	effective device figure of merit ( $\text{K}^{-1}$ )

### Greek symbols

$\kappa$	thermal conductivity ( $\text{W}\cdot\text{m}^{-1}\cdot\text{K}^{-1}$ )
$\mu$	dynamic viscosity ( $\text{kg}\cdot\text{m}^{-1}\cdot\text{s}^{-1}$ )
$\rho$	electric resistivity ( $\Omega\cdot\text{m}^{-1}$ ), density ( $\text{kg}\cdot\text{m}^{-3}$ )
$\sigma$	electrical conductivity ( $\text{m}\cdot\Omega^{-1}$ )
$K$	lumped conductivity ( $\text{W}\cdot\text{m}^{-1}\cdot\text{K}^{-1}$ )

### Subscripts

$c$	cold side, cooling
$exp$	experimental
$GS$	Goldsmid's method
$h$	hot side, heating

<i>i</i>	inlet
<i>l</i>	electrode resistance
<i>max</i>	maximum
<i>n</i>	n-type node
<i>o</i>	outlet
<i>p</i>	p-type node
<i>s</i>	side
<i>sim</i>	simulation
<i>test</i>	empirical method
<i>w</i>	water
<i>0</i>	initial testing

## 1 INTRODUCTION

Thermoelectric (TE) cooling has seen rapid developments since the basic science of TE materials became well established [1]. The most popular approach to applying TE technologies is through TE modules, which are compact in size and light in weight [2]. A typical TE module consists of a bunch of thermocouples made of n-type and p-type materials wired together. The pi-type modules, as shown in Figure 1, have the advantages of low cost, modularity, simple design, and environmental friendliness [3]. A TE module is usually consisted of two ceramic substrates, multiple n-p node couples (pairs), and connected metal joints. Apart from electronics cooling [4–7], there has been growing interest in applying TE modules for refrigerators [8–10], personal thermal comfort [11], dishwashers [12], and clothes dryers [13,14].

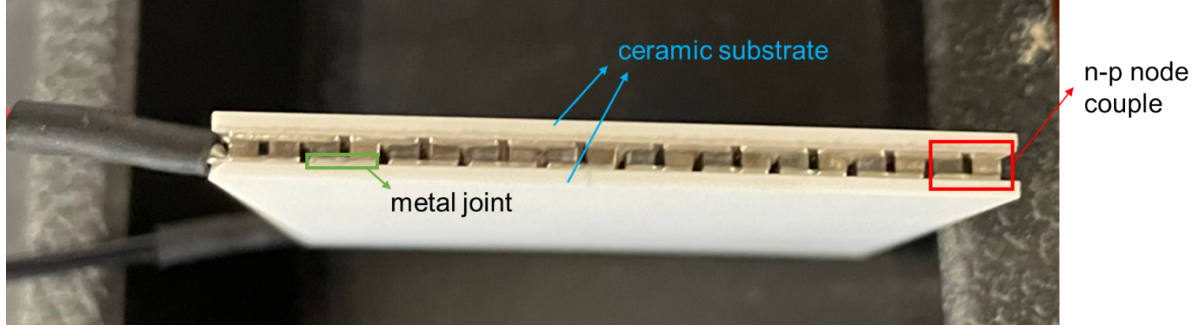


**Figure 1 Typical 127-node 40mm\*40mm pi-type thermoelectric module**

TE physical parameters (Seebeck coefficient  $s$ , thermal conductivity  $\kappa$  and thermal resistance  $\rho$ ) are important variables but actual values are difficult to quantity due to the dynamic changing of temperature ( $T$ ) when TE modules work normally. The true one-dimensional temperature distribution along a TE element is described by Eq. 1, which is the one-dimensional differential equation for energy conservation along a TE element.  $A$  represents the area of the element, and  $I$  represents the current passing through the element. At this point, this equation contains no simplifying assumptions other than neglecting heat loss along the element.

$$\frac{d}{dx} \left[ \kappa(T) A \frac{dT}{dx} \right] \pm IT \frac{ds}{dT} \frac{dT}{dx} + \frac{I^2}{A} \rho(T) = 0 \quad (1)$$

Eq. 1 shows that all material properties and temperatures are functions of the temperature along of the TE element. Since the temperature is a function of the length ( $x$ ) along the node, the material properties are functions of  $x$  as well. In this equation, the first term on the left side represents Fourier's heat conduction, the second term denotes the Thomson heating, and the third term is internal heat source caused by Joule heating.

Due to the fact that the single TE module is comprised of multiple TE n-p node couples, other than  $s$ ,  $\rho$ , and  $\kappa$ , the overall electric resistance  $R$ , lumped thermoelement thermal conductivity  $K$ , and lumped Seebeck coefficient  $S$  of a single TE module are widely used to evaluate the TE module thermodynamic performance [15].  $s$ ,  $\rho$ , and  $\kappa$  are linked with  $S$ ,  $R$ , and  $K$  by Eq. 2 to Eq. 4 if n and p nodes share the same materials. This assumption also implies that all node pairs are homogeneous and share the same properties, a deduction process detailed in Goldsmid's book [15]. Additionally, other studies [16,17] further explore the nature of the Peltier Effect, providing valuable references for interested readers.

$$S = N \cdot s_i = N \cdot (s_p - s_n) \approx N \cdot 2s \quad (2)$$

$$R = N \cdot R_i = N \cdot \left( \frac{l_n \rho_n}{A_n} + \frac{l_p \rho_p}{A_p} + R_l \right) \approx \frac{N^2 l}{A_f} 4\rho \quad (3)$$

$$K = N \cdot K_i = N \cdot \left( \frac{A_n \kappa_n}{l_n} + \frac{A_p \kappa_p}{l_p} \right) \approx \frac{Af}{l} \kappa \quad (4)$$

where  $N$  is the n-p node couple numbers<sup>2</sup>;  $A$  is the module area;  $f$  is the fill factor; and  $l$  and  $A$  with n or p subscript are the geometry parameters of the nodes;  $R_l$  is the electrode resistance including the contact resistance per couple. By using the lumped property parameters, the capacity equation (Eq. 1) can be rewritten as Eq. 5 to calculate the overall cooling capacity of one TE module.

$$Q_c = SIT_c - K(T_h - T_c) - I^2 R/2 \quad (5)$$

$$Q_h = SIT_h - K(T_h - T_c) + I^2 R/2 \quad (6)$$

$$U = SI(T_h - T_c) + IR \quad (7)$$

Extracting the property parameters, especially the lumped parameters, is significant in designing an energy system using TE modules, since the capacity can be estimated straight forward using Eq. 5 [15].

Since  $s$ ,  $\rho$ , and  $\kappa$  are all functions of  $T$ , the most reasonable and accurate method to extract the material property parameters is using the performance tables summarized from material studies (refer to section 2.1 and attached database) or performance curves derived from the tables. Then using Eq. 1 to solve the temperature distribution  $T(x)$  along the TE node with boundary conditions at  $x = 0$  and  $x = l$  (hot side and cold side surface conditions). However, this differential equation is extremely complicated; plus, TE material property tables (curves) may not be always available. A large number of commercial bismuth telluride ( $\text{Bi}_2\text{TE}_3$ ) family TE modules exist on the market [16]. Different TE module manufactures may use different materials in the  $\text{Bi}_2\text{TE}_3$  family. TE modules' specification from the vendors usually do not mention the detailed materials (e.g., mentioning  $\text{Bi}_2\text{TE}_3$  but not mentioning the  $y$  and  $z$  numbers of  $\text{Bi}_{2-y}\text{Ge}_y\text{Te}_{3-z}\text{Se}_z$  or not mentioning if it is doped with Cu). Ignoring these differences could bring up to 100% property differences (refer to [22–25] and Appendix 1). Thus, it's not practical to search the properties online or in the literatures.

Extracting the lumped properties from manufacture's datasheet is a simple and reasonable substitute methods [26]. Cai et al. [26] conducted a comprehensive review on current simplified formulas of TE physical parameters. They compared six different formulas and found the formulas (refer to Eq. 14 to Eq. 16) using vendor's data points tested when cooling capacity is zero and when cooling capacity reached maximum value had the best performance [26]. Though Cai et al. [26] grouped the references in one case, the models used by [21] (Eq. 17 to Eq. 19) and [19,27] (Eq. 14 to Eq. 16) were different. Recent years, some researchers also proposed other format formulas [28].

In light of the limitations identified in the existing body of research, this study seeks to address several critical gaps. These include: (1) the lack of comparative analysis between prevalent formulae; (2) the reliance on potentially inaccurate vendor-supplied data for model development [29], with evidence suggesting that vendor datasheets could overstate TE module performance by 10-20% [30]; (3) the disregard for the fundamental assumption that temperature differentials should be minimal and the absence of information concerning the applicable range for reported formulae; and (4) an omission of guidelines for extracting TE properties from experimental data.

To address these gaps, the present study aims to: (1) compare three existing formulae using vendor datasheets and establish the applied range and basic assumptions of each formula; and (2) design a laboratory test facility for the validation and refinement of the model through experimental investigations.

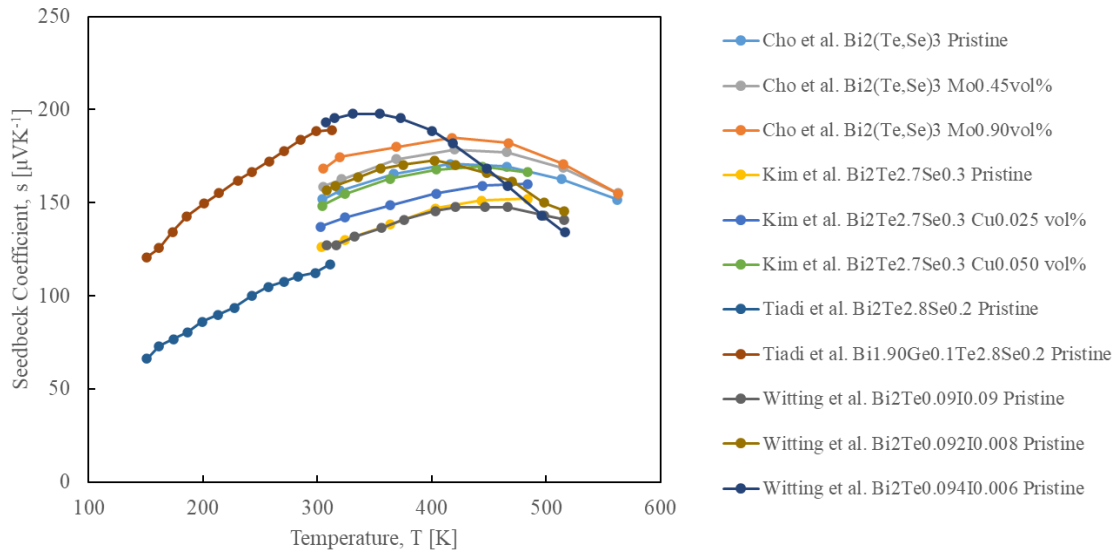
---

<sup>2</sup> If  $N$  stands for the node number, the formula should be revised as  $S = Ns$  and  $R \approx \frac{N^2 l}{Af} \rho$ . The reference [18] used these revised formulas but mistakenly referred to  $N$  as the number of thermocouples, which is believed to be a typographical error when compared to other references [19,4,5,20–22].

In this study, the workflow consists of discussing three methods for extracting TE module property parameters: firstly, by leveraging material properties available in existing literature; secondly, by utilizing property extraction formulae as summarized in scholarly works; and lastly, by conducting laboratory tests that include indirect heat flux measurements. Each method is scrutinized for its benefits and associated risks. Upon completion of this comparative analysis, the study will put forth a recommended strategy aimed at assisting future researchers and engineers in the accurate extraction of TE properties. The novelty of this study lies in several key contributions: (1) the execution of experimental work in a laboratory setting to validate the model and elucidate its limitations; (2) the highlighting of potential risks; (3) the clarification of possible assumptions from both material and engineering perspectives; (4) the consideration of temperature differential impacts; and (5) a comprehensive summary of data extraction procedures for future researchers and engineers.

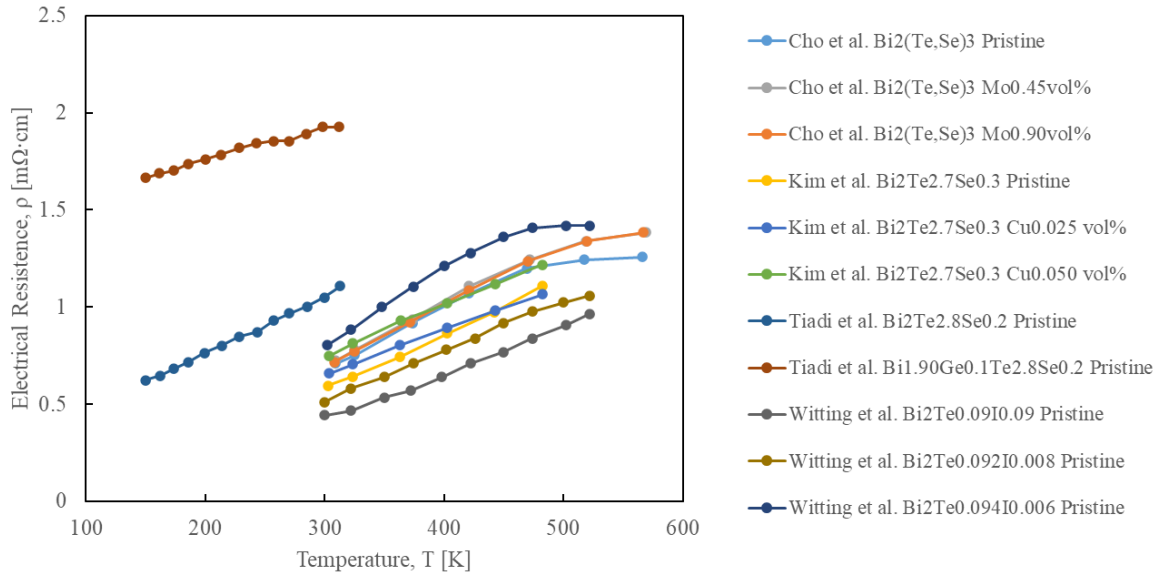
## 2 MATERIAL CHARACTERIZATION APPROACH

The authors conducted a literature survey to collect reported  $\text{Bi}_2\text{Te}_3$  family materials properties at different temperatures. The reference's data was used to plot Figure 2 [22–25]. The detailed data was attached in the database.

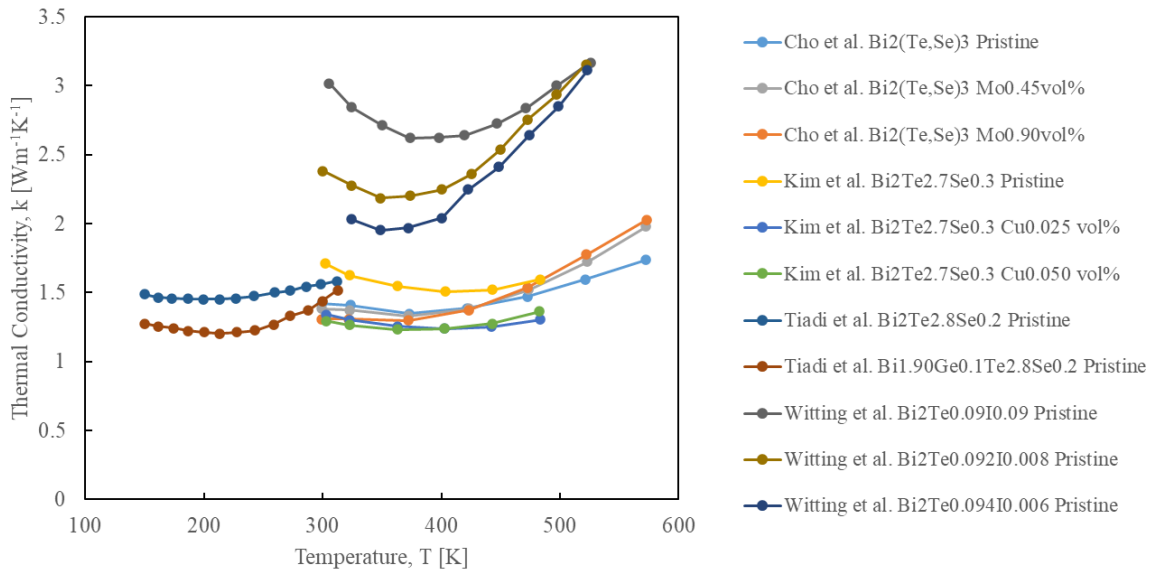


a) <sup>3</sup>Seebeck coefficient  $s$

<sup>3</sup> p-type materials were listed, and the absolute values were plotted.



b) Electric resistance  $\rho$



c) Thermal conductivity  $\kappa$

**Figure 2 Bismuth telluride materials properties reported in the literature**

Figure 2 illustrates the relationship between properties and temperature for different materials in bismuth telluride families. At 300 K, discrepancies among Bi<sub>2</sub>Te<sub>3</sub> materials can reach up to 39.3%, 76.8%, and 57.0% for  $s$ ,  $\rho$ , and  $\kappa$ , respectively. Consequently, it is evident that an empirical equation applicable to one module may not be suitable for another.

A comparison of the properties between 300 K and 340 K reveals that  $s$  exhibits a maximum variation of 4.5%, while  $\rho$  and  $\kappa$  change up to 25% and 9%, respectively. Consequently, it is reasonable to assume that the  $s$  is not temperature-dependent within the room temperature range. However, this assumption cannot be extended to  $\rho$  and  $\kappa$ , implying that  $R$  and  $K$  are functions of temperature.

### 3 MODELING APPROACHES

#### 3.1 Survey of existing formulas

##### 3.1.1 Weera et al.'s method

Weera et al. [28] proposed a method to estimated TEC effective material properties (Eq. 38-42 in the reference). This method was cited and used by [29,31–34]. In fact, this method is close to the approach proposed by Luo [19] in 2008 (Eq. 23-25 in the reference). The characteristic of this approach is to extract the properties by only using  $\Delta T_{max}$ ,  $I_{max}$ , and  $Q_{max}$  without  $U_{max}$  (these metrics are commonly given by the manufacture's specification;  $I_{max}$  stands for the current that achieves the maximum  $\Delta T$ ;  $U_{max}$  is the voltage at  $I_{max}$ ;  $Q_{max}$  is the maximum amount of heat that can be transferred or removed from the cold side to the hot side of the TE module). The equations can be written as shown by Eq. 8 to Eq. 11.

$$S = \frac{2Q_{max}}{I_{max}(T_h + \Delta T_{max})} \quad (8)$$

$$Z = \frac{2\Delta T_{max}}{(T_h - \Delta T_{max})^2} \quad (9)$$

$$R = \frac{(T_h - \Delta T_{max})S}{I_{max}} = \frac{2Q_{max}(T_h - \Delta T_{max})}{I_{max}^2(T_h + \Delta T_{max})} \quad (10)$$

$$K = \frac{S^2}{RZ} = \frac{(T_h - \Delta T_{max})Q_{max}}{(T_h + \Delta T_{max})\Delta T_{max}} \quad (11)$$

Weera et al. [28] deducted Eq. 12 from Eq. 5 (Eq. 33 in the reference).

$$\Delta T = \frac{1}{K} \left( ST_c I - \frac{1}{2} I^2 R \right) \quad (12)$$

Weera et al. [28] calculated the derivative of the temperature difference ( $\Delta T$ ) with respect to the current of the Eq. 12 and set it zero to calculate  $I_{max}$  as shown by Eq. 13.

$$\frac{d\Delta T}{dI} = \frac{1}{K} (ST_c - IR) = 0 \quad (13)$$

However, this deduction relies on several assumptions that were not only overlooked by Weera et al. [28] but also by studies citing their work [29,31–34]. These assumptions include: (1) the Seebeck coefficient ( $S$ ) is independent of current ( $I$ ); (2) overall electric resistance ( $R$ ) is not a function of current ( $I$ ); and (3) hot side temperature ( $T_h$ ) is not a function of current ( $I$ ). Assumption 1 might be acceptable, as the  $S$  can be treated as a constant [35]. However, assumption 2 is only valid when the temperature difference ( $\Delta T$ ) is small. Assumption 3 may not be reasonable in several practical cases where  $T_c$  drops sharply (i.e.,  $\Delta T$  should be small). Some ones may argue that  $\Delta T$  is relied on  $T_h$  since as the current ( $I$ ) increases, the hot side temperature of the TE cooler will rise, and the cold side temperature will decrease. This occurs when the thermal mass of the cold side is small, and heat transfer resistance is large. However, when load exists (e.g., water or air is passing through TE surfaces),  $\Delta T$  and  $T_h$  can be independent.

##### 3.1.2 Luo's method

This method was first reported by Lineykin and Ben-Yaakov in 2005 [27] and later summarized by Luo [19] in 2007. Compared with Weera et al.'s approach [28], this method uses  $\Delta T_{max}$ ,  $I_{max}$ , and  $U_{max}$  without  $Q_{max}$ .

$$S = \frac{U_{max}}{T_h} \quad (14)$$

$$R = \frac{(T_h - \Delta T_{max})U_{max}}{T_h I_{max}} \quad (15)$$

$$K = \frac{(T_h - \Delta T_{max})U_{max}I_{max}}{2T_h \Delta T_{max}} \quad (16)$$

The deduction process is also similar to Weera et al.'s approach [28]. Thus, this method is also based on the assumptions that  $S$ ,  $R$ ,  $T_c$  is not a function of  $I$ . Thus, this approach has the same limitation as Weera's approach.

### 3.1.3 Chen and Snyder's method

Chen and Snyder's method [21] was also cited a lot (e.g., [6,18,26,36–38]) and could be written as from Eq. 17 to Eq. 19 (Eq. 24-Eq.26 in the reference [21]).

$$S = \frac{2Q_{max}(T_h - \Delta T_{max})}{T_h^2 I_{max}} \quad (17)$$

$$R = \frac{2(T_h - \Delta T_{max})^2 Q_{max}}{T_h^2 I_{max}^2} \quad (18)$$

$$K = \frac{(T_h - \Delta T_{max})^2 Q_{max}}{T_h^2 \Delta T_{max}} \quad (19)$$

When comparing this method to Weera et al.'s approach [28], a ratio factor  $\frac{(T_h - \Delta T_{max})^2}{T_h^2}$  exists. In fact, this difference is due to the fact that Chen and Snyder changed  $T_h$  to  $T_h - \Delta T_{max}$  in the following equation (Eq. 19 and Eq. 23 in the reference [21]).

$$Q_{max} = \frac{Af}{l} \frac{\alpha^2 T_h^2}{2\rho} \quad (20)$$

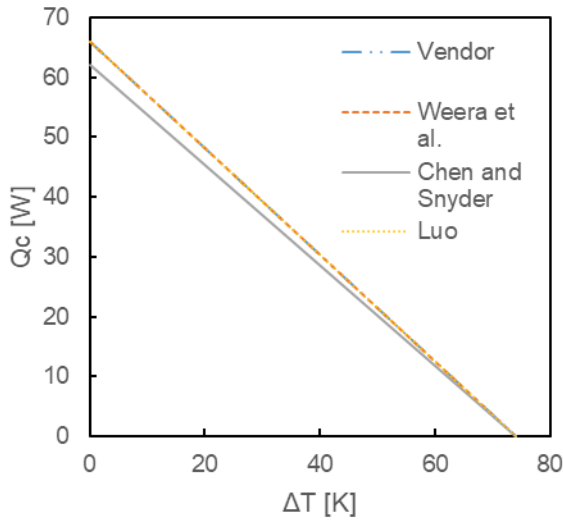
This change is based on their assumption that usually in the tests,  $T_h$  is changing while  $T_c$  is always kept as constants; they also assume the current is kept at  $I_{max}$ . Thus, the application is quite different from the other two models. This divergence arises from their underlying assumptions that, typically in experiments,  $T_h$  varies while  $T_c$  remains constant; they also assume that the current is maintained at  $I_{max}$ . Consequently, the applicability of their model differs significantly from the other two models under consideration.

## 3.2 Compare the properties extraction formulas

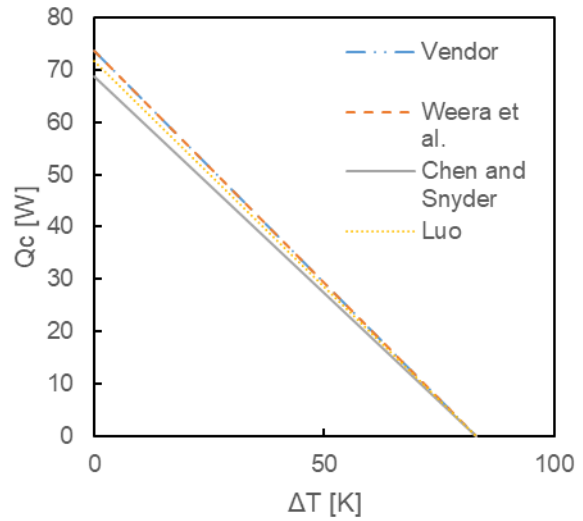
The three methods were compared with vendor's datasheet. The module used is “inbTC1-12706”<sup>4</sup>.

---

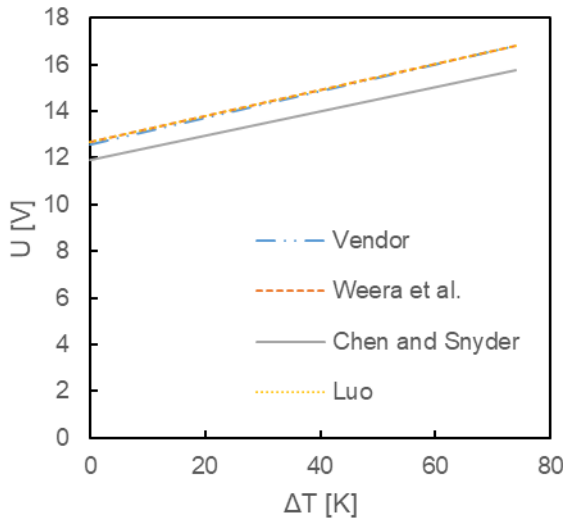
<sup>4</sup> This paper mainly focused on “inbTC1-12706” samples. Another type of modules “VT-199-1.4-0.8” were tested and the data was listed in the appendix.



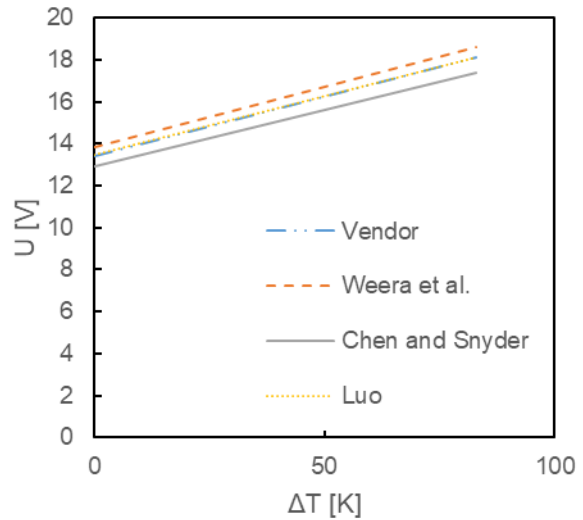
a)  $Q_c$  vs.  $\Delta T$ ,  $T_h = 27$  °C



b)  $Q_c$  vs.  $\Delta T$ ,  $T_h = 50$  °C



c)  $U$  vs.  $\Delta T$ ,  $T_h = 27$  °C



d)  $U$  vs.  $\Delta T$ ,  $T_h = 50$  °C

**Figure 3 Different models comparisons with vendor's datasheet**

Figure 3 shows the cooling capacity and voltage values from eq. 5 to eq. 6 by substituting the predicted lumped properties ( $S$ ,  $R$ , and  $K$ ). Data from the vendor's datasheet is added as the reference (in the Appendix 4).

The results indicate that Luo's model is unable to accurately predict the capacity at  $T_h = 50$  °C, but performs well in other cases. In contrast, Weera et al.'s model fails to match the voltage at  $T_h = 50$  °C, yet demonstrates satisfactory performance in other instances. This outcome aligns with the observation that Weera et al. incorporated  $Q_{max}$  in their equations, while Luo employed  $U_{max}$  in their calculations.

As the findings, Luo's model fails to match the capacity at  $T_h = 50$  °C, but matches other cases well. Weera et al.'s model cannot match the voltage at  $T_h = 50$  °C, but matches other cases good. This result is consistent with the fact that Weera et al. used  $Q_{max}$  in their equations while Luo used  $U_{max}$  in the equations. Chen and Snyder's method has some gaps for each case (6.1% on  $Q_c$  and 6.5% on  $U$ ), since in our cases,  $T_h$  remains constant while  $T_c$  varies, which deviates from their original assumptions.

### 3.3 Summary

Based on the analysis, the authors recommend opting for either Luo's or Weera et al.'s method when experimental validation of the module's performance is unavailable and the temperature change is minimal on the hot side but substantial on the cold side. Conversely, Chen and Snyder's method is advised when there is a significant temperature change on the hot side but minimal change on the cold side.

## 4 EXPERIMENTAL APPROACH

In this section, we outline an experimental framework aimed at indirectly assessing the heat flux of TE modules for the purpose of property estimation. The setup employs two bundles of copper tubes positioned on either side of the TE modules. By monitoring the enthalpy change of the fluid flowing through these tubes, we are able to calculate the heat flux.

### 4.1 Thermoelectric heat pump assembling

In order to validate the TE module performance, a TE Heat Pump (TEHP) was assembled with capillary tubes and TE modules. The core approach involves channeling a fluid past the surface of the TE module and quantifying the change in enthalpy of the fluid as a means to indirectly ascertain the heat flux generated by the TE modules.

$$Q_h = MFR_h(c_p(T_{h,o})T_{h,o} - c_p(T_{h,i})T_{h,i}) \quad (21)$$

$$Q_c = MFR_c(c_p(T_{c,i})T_{c,i} - c_p(T_{c,o})T_{c,o}) \quad (22)$$

where  $c_p$  represents the specific heat of water at a given temperature,  $T$  denotes the temperature of the water,  $MFR$  stands for the mass flow rate of the water, and  $Q$  is the measured capacity.

The material used is listed in the Table 1. We tested two types of TE modules from different manufactures. The test results of one type “inbTC1-127.06” are detailed in the manuscript while the results of another type “VT-199-1.4-0.8” is listed in the Appendix 3 for reference.

**Table 1 Material used**

Items	Manufacture	Geometry parameters
Thermoelectric module	W*** inbTC1-127.06	40 mm*40 mm*3.2 mm
Capillary tubes	JB INDUSTRIES	2.54 mm in ID, and 4.00 mm in OD  400 mm length
Header tubes	JB INDUSTRIES	9.5 mm-ID
Thermal paste	UNIWELD	-

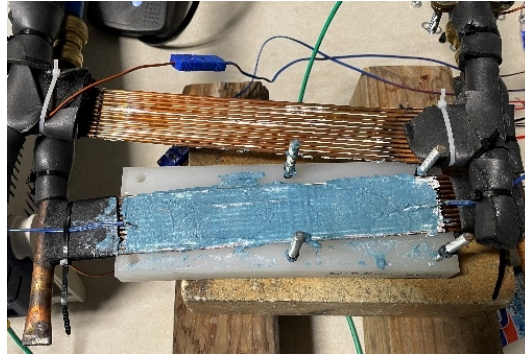


**Figure 4 Thermoelectric heat pump assembling**

Capillary tubes were put in parallel, and the larger 9.5 mm-ID header tubes were used as headers. The total capillary tube length is 400 mm, which is much larger than the entrance tube length and can guarantee the fluid is fully developed in the tube bundles. Compared with other regular tubes [39,3,12], this design can improve the heat transfer between the fluid and the TE surfaces. 5 TE modules were set in parallel as well in the capillary tubes. We used water as the working fluid to validate the performance of the assembled TEHP sample.

#### 4.2 Test facilities

We use DC power supply as the power source and to measure voltage and current. A water heater was used to supply hot water and the cold side inlet water was city water. Figure 5 shows the validation test facility, where eight thermocouples were placed to measure the hot water inlet/outlet, cold water inlet/outlet, hot tubes inlet/outlet surface, and cold tubes inlet/outlet surface temperatures.

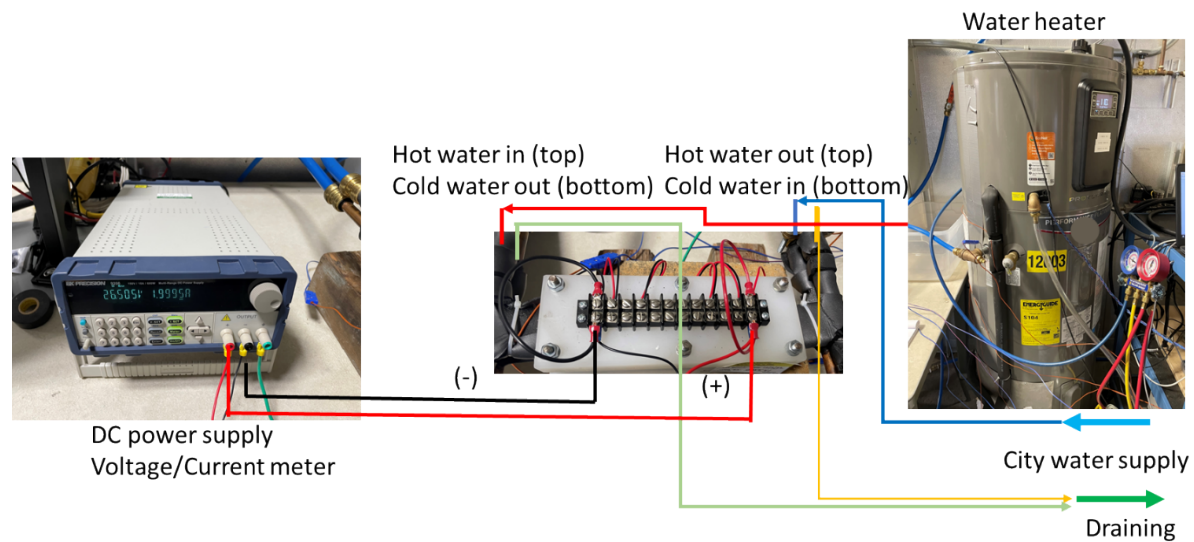


**Figure 5 Thermoelectric heat pump test facility**

The uncertainties of the measurements are detailed in Table 3.

**Table 2 Uncertainties of measured quantities**

Quantity	Instrument	Uncertainty
Geometry	Vernier Caliper	$\pm 0.02$ mm

Temperature	Type T thermocouple	±0.5 °C
Mass flow rate	Coriolis flowmeter	±0.5%
Applied voltage to TE banks	Multi-Range DC Power Supply	±2 V
Current through TE banks	Multi-Range DC Power Supply	±0.05 A
Capacities	Derived quantity	±0.5 W
UA values	Derived quantity	±1 W/K

The power source used is “BK PRECISION 9200B Series Multi-Range DC Power Supply.” It can also be used to measure the voltage and current through the TE modules. Rheem’s water heater was used to supply hot water. The cold side inlet water is the city water.

### 4.3 Thermoelectric module properties

In our tests, we used the lumped temperature (average temperature) of the TEHP two sides to stand for  $T_h$  and  $T_c$ .

#### 4.3.1 Seebeck Coefficient ( $S$ )

When no external power source was connected to the TEHP and there was a temperature difference between its two sides, the TE modules worked as generators. The voltage (also known as the Seebeck Voltage) generated by the temperature difference can be given as:

$$V = S(T_h - T_c) \quad (23)$$

In our study, we added thermal paste between the tube layers and TE module layer. The contact thermal resistance and the thermal resistance from conduction were much smaller than the convection resistance from water to tube walls. Thus, the average temperatures at the two ends of the tubes were used to represent the hot and cold surface temperature and to calculate the temperature difference. Figure 4 shows the measurements. As the temperature lift increased, the Seebeck voltage was a bit larger than the predicted value. This is consistent with research that the Seebeck voltage will slightly increase as the temperature increases. There was a 5% error at a 15-K-temperature lift. Therefore, it is reasonable to consider  $S$  to be a constant in our study. Since we used 5 modules, the Seebeck coefficient is:

$$S_{exp} = 0.0411 \text{ [V/K]} \quad (24)$$

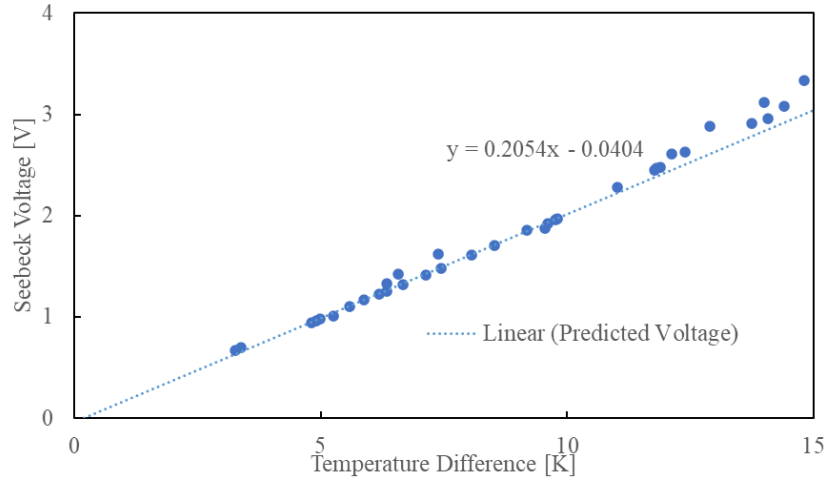


**Figure 6 Seebeck voltage measurement**

We can also find that the slope start increases when the temperature difference increase. This finding is consistent with Figure 2, which shows that most materials' Seebeck coefficient increase with temperature from the literature.

#### 4.3.2 Electric Resistance ( $R$ )

Another parameter which can determine the heating and cooling capacities are the electric resistance of the modules. From the literature, it should be relied on the hot and cold surface temperature of the TE modules. The electric resistance ( $R$ ) can be given by:

$$R = \frac{V - S(T_h - T_c)}{I} \quad (25)$$

$V$  is the measured voltage value, and  $I$  is the measured current value.

We plotted the values in Figure 7.  $\Delta T$  was dependent on  $T_h$  in this test (as  $T_h$  increased  $\Delta T$  increased) since the city water was used as the inlet of the cold side. The cold side surface temperature varied from 16 °C to 19 °C for all test points.

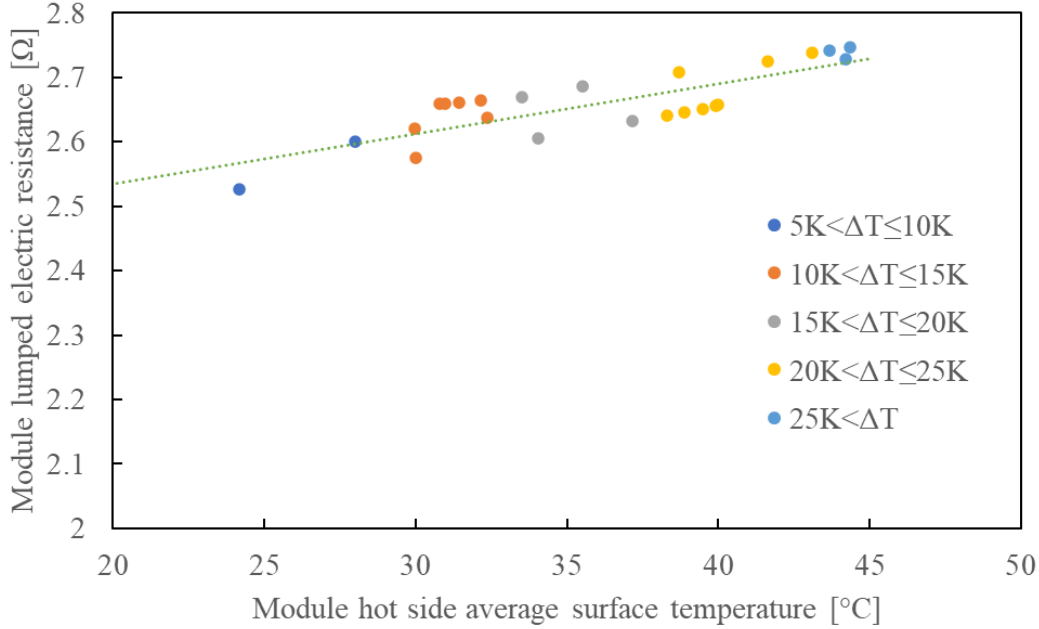


**Figure 7 Electric resistance measurement**

From the tests, we can calculate the electric resistance around our test range is:

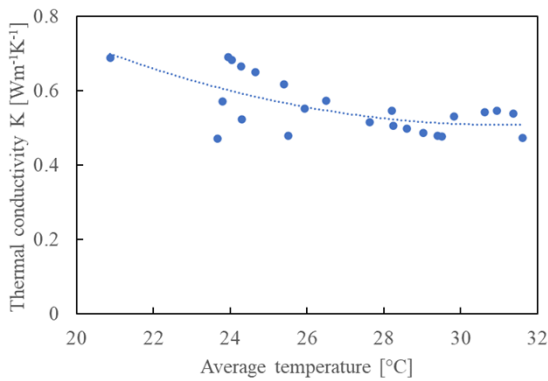
$$R_{exp} = 2.5 \sim 2.8 \text{ } [\Omega] \quad (26)$$

We also used resistance meter to measure the value under room temperature (around 20 °C). The value is around 2.4~2.5 Ω.

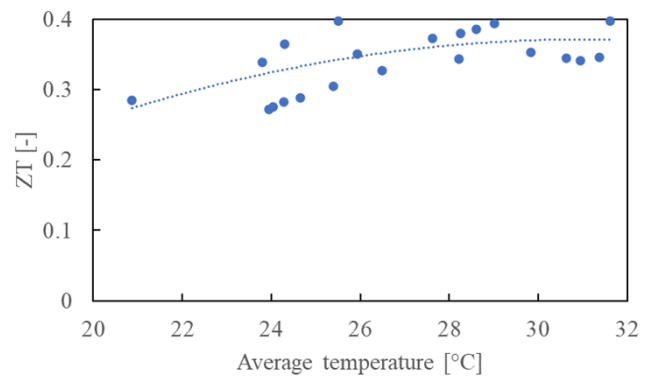
### 4.3.3 Thermal conductivity ( $K$ ) and $ZT$

Thermal conductivity can be calculated by eq. 27, which can be derived by adding eq. 5 and eq. 6:

$$K = \frac{SI(T_h + T_c) - (Q_h + Q_c)}{2(T_h - T_c)} \quad (27)$$



a)  $K$  vs. Ambient temperature



b)  $ZT$  vs. Ambient temperature

**Figure 8 Measured thermal conductivity and ZT**

$$ZT = \frac{S^2 T}{RK} \quad (28)$$

The  $ZT$  value can be computed using Eq. 28. To illustrate the trend, two second-order polynomial curves are plotted. As the temperature ranges from 300 K to 400 K, the  $K$  values decrease and approach a minimum point, while the  $ZT$  values increase and approach a maximum point. This observed pattern is in line with the trends reported in the literature [22].

#### 4.3.4 Summary

Table 3 shows a comparison between vendor's data and the measured data. In the observed temperature differences (15-K), the  $S$ ,  $R$ , and  $K$  values changed by 0.3%, 6%, and 5%, respectively. These differences will result in 0.4%, 6%, and 4% variations in the cooling capacity calculation (assuming  $T_c$  to be 20°C and  $I$  to be 2 A). Consequently, it is reasonable to consider  $S$  as a constant. For large-scale systems (e.g., dryer [14]), the errors from other components could be larger than 10%. Hence, it is also reasonable to assume that the  $R$  and  $K$  values remain constant in system-level modeling [40].

In addition, we compare the vendor's data obtained through the extraction method with the measured values. We did not compare the results under the exact same conditions since the vendor's data only provide the points at  $T_h = 27$  °C and  $T_h = 50$  °C, and these two conditions did not occur in the tests. We found that, except for  $K$ , the  $S$  and  $R$  values deviated significantly from the vendor's data, causing the performance ( $ZT$ ) to be only half of the vendor's report. Variations in the properties can result in a 40% discrepancy in the estimation of cooling capacity.

Moreover, although the  $R$  values are incorrect, the increase in  $R$  value from 27°C to 50°C from the prediction is close to the measured values. This suggests that the resistance value can be corrected using a linear function with just one tested point. One can assume the  $R$  value predicted through the model (either Weera's or Luo's) at 27°C is  $R_1$ , and at 50°C is  $R_2$ , the temperature difference  $\Delta T_{2,1} = 23$  K. If one can measure the resistance at a given hot side temperature  $T_0$  in the range 27~50 °C, the resistance caused by the cold side temperature variation could be corrected as follows:

$$R = R_0 + \frac{R_2 - R_1}{\Delta T_{2,1}}(T_0 - T_1) \quad (29)$$

**Table 3 Comparison between vendor's data and measured data**

	Weera's method		Luo's method		Chen and Snyder's method		Measured data	
	27	50	27	50	27	50	28	44
$T_h$ [C]	27	50	27	50	27	50	28	44
$S$ [V/K]	0.056	0.058	0.056	0.056	0.053	0.054	0.041	0.041
$R$ [ $\Omega$ ]	2.01	2.19	2.01	2.13	1.89	2.05	2.60	2.75
$K$ [ $\text{Wm}^{-1}\text{K}^{-1}$ ]	0.54	0.52	0.54	0.51	0.51	0.49	0.56	0.53
$ZT$ [-]	0.76	0.81	0.76	0.81	0.76	0.81	0.35	0.37

#### 4.4 Heat transfer analysis

We calculated the  $UA$  values using the measured data as shown by Table 4 (detailed experimental data were attached in Appendix 2). The  $UA$  values can be accessed through the following equations by giving the capacity:

$$Q = UA \cdot LMTD = UA \frac{\Delta T_A - \Delta T_B}{\ln(\Delta T_A) - \ln(\Delta T_B)} \quad (30)$$

We used the data with 4-A current to validate  $UA$  since at this time the capacity was maximized, and the error could be the smallest.

**Table 4 Measured  $UA$  values (MFR = 0.04 kg/s).**

MFR [kg/s]	UA hot [W/K]	UA cold [W/K]	Average Hot side water Temp. [°C]	Average Hot surf. Temp. [°C]	Average Cold side water Temp. [°C]	Average Cold surf. Temp. [°C]
0.04	43.48	36.02	27.36	35.78	21.25	18.07
0.04	43.95	36.70	29.21	37.35	21.30	18.30
0.04	44.17	37.23	30.02	37.98	21.31	18.40
0.04	45.23	38.62	31.80	39.53	21.35	18.63
0.04	45.57	39.05	33.67	41.21	21.43	18.87
0.04	45.54	42.09	35.13	42.41	21.48	19.05
0.04	46.99	41.13	36.41	43.48	21.54	19.23
0.04	47.39	41.89	37.51	44.51	21.58	19.35
0.04	47.81	42.86	38.19	45.11	21.59	19.47

In order to estimate  $UA$ , the heat transfer coefficient between the fluid and the inner surface of the channel was predicted using the Dittus-Boelter correlation [41]. Given the small tube bundle diameters and relatively long tube lengths, the flow was considered fully developed and not laminar. For various fluid regimes and channel geometries, alternative suitable correlations can be employed to predict the heat transfer coefficient.

$$Nu = 0.023Re_D^{4/5} Pr^n \quad (31)$$

$$Pr = \frac{c_p \mu_w}{k_w} \quad (32)$$

$$Re = \frac{\rho_w u D}{\mu_w} \quad (33)$$

$\mu_w$  is the dynamic viscosity of water and is a function of water temperature.  $u$  is the water flow speed and can be calculated from  $m_h$  and  $m_c$ .  $c_p$  is the specific heat of water,  $k_w$  is the thermal conductivity of water,  $D$  is the characteristic linear dimension,  $Re$  is the Reynolds number,  $Pr$  is the Prandtl number; and  $Nu$  is the Nusselt number. When hot side inlet water temperature equals 37 °C and cold side inlet temperature equals 21 °C, hot side  $Re$  equals 2879,  $Pr$  equals 4.87,  $Nu$  equals 22.81, and  $HTC$  (Heat Transfer Coefficient) equals 7375.

The  $UA$  values for each segment, calculated using the correlations, are 10.73 W/K (hot side) and 8.95 W/K (cold side). In comparison to the measured data, the predicted  $UA$  for the hot side is 12% larger, while the cold side prediction is 4% larger. These results align with our assumption regarding the non-laminar flow. Utilizing capillary tubes reduces the entrance length, hindering the flow from fully developing and leading to a non-laminar flow. Consequently, the heat transfer coefficient becomes five times greater than with larger tubes. The last row of data in Table 3 was used to estimate the capacity, resulting in predicted heating and cooling capacities of 267.5 W and 67.5 W, respectively. The measured capacities were 266.3 W and 79.2 W.

#### 4.5 Estimate property data from experiments

Although conducting multiple tests to generate performance curves for TE modules may seem like a practical solution, it is often labor-intensive. Furthermore, our study, along with existing literature [30], indicates that manufacturer-provided data can be unreliable. Consequently, a methodology for estimating TE module properties from experiments holds significance. Despite the utility of such an approach, scant literature elaborates on this, prompting us to summarize it herein for the benefit of the readers.

First, the user must have access to testing facilities to measure the cooling or heating capacity. The user then needs to conduct an initial test (denoted by the subscript “0”) with  $I_0$  current and measure the hot side temperature ( $T_{h0}$ ), the cold side temperature ( $T_{c0}$ ), voltage ( $V_0$ ), and capacity (e.g., cooling capacity  $Q_{c0}$ ). Subsequently, the user needs to cut off the power source and measure the voltage (i.e., Seebeck voltage  $V_{s0}$ ). Table 5 summarizes this data.

**Table 5 Required tested values**

Test	Current	Hot side [K]	Cold side [K]	Voltage	Capacity
1	$I_0$	$T_{h0}$	$T_{c0}$	$V_0$	$Q_{c0}$
2	0	$T_{h0}$	$T_{c0}$	$V_{s0}$	-

Then, the properties can be extracted through the following equations:

$$S_0 = \frac{V_{s0}}{T_{h0} - T_{c0}} \quad (34)$$

$$R_0 = \frac{V_0 - S(T_{h0} - T_{c0})}{I_0} \quad (35)$$

$$K_0 = \frac{ST_{c0}I_0 - \frac{1}{2}I_0^2R - Q_{c0}}{(T_{h0} - T_{c0})} \quad (36)$$

The electrical resistance  $R_0$  can be adjusted using eq. 29 if  $\Delta T$  is considered non-negligible.

### 5 RECOMANDED DATA EXTRACTION APPROACH

In summary, this paper presents comprehensive analysis for comparing existing models and recommend the best approach for future engineers and researchers to develop thermoelectric-related energy system models and design associated systems. The following steps are suggested:

1. Verify the availability of detailed material information (e.g.,  $\text{Bi}_2\text{Te}_{2.7}\text{Se}_{0.3}$  Cu 0.025vol%; merely specifying  $\text{Bi}_2\text{Te}_3$  is insufficient). If the material composition is known, properties can be extracted using the performance curves provided in the literature (e.g., Figure 2).
2. Evaluate the availability of testing facilities to determine whether the capacity of the TE modules can be measured. Measurements can be taken either directly (e.g., using a heat flux meter) or indirectly, as outlined in this paper. If feasible, the methodology proposed in Section 4.3 can be utilized to acquire the properties of the TE modules. However, it is critical to ensure that the temperature range on both the hot and cold sides falls between 20°C and 50°C; otherwise, performance cannot be guaranteed.
3. Examine the accessibility of vendor datasheets. Users may opt for Weera’s or Luo’s approach to extract properties. However, it is essential to note that these approaches require small  $\Delta T$  (based on the results of this study, a 15 K threshold is recommended). Readers should also be aware that vendor data can be inaccurate, potentially leading to deviations larger than 40% in capacity estimation.
4. If vendor datasheets are unattainable, measuring performance curves or tables remains the only option. Readers may refer to empirical models found in references [42,3,43] for guidance.

In our manuscript, we elucidate the rationale behind the selection of temperature ranges for our study, drawing from three distinct methodologies for parameter extraction in compact thermoelectric modules. Specifically, Figure 2, which is based on material properties, illustrates a broad temperature range from 100 K to 400 K. This wide range is achievable due to the depth of material studies that explore extensive temperature differences under varied conditions. In contrast, Figure 3 utilizes data based on vendors' specifications, presenting a narrower temperature change spectrum from 0 K to 70 K, indicative of the more limited scope typical of empirical methods reliant on secondary data from other researchers or manufacturers. Our experimental parameters, particularly the temperature difference range from 0 K to 15 K, are determined by the capabilities of our water tank setup, which is designed to supply hot water. This setup inherently restricts us to a maximum temperature differential of 15K. Moving forward, our objective is to broaden our experimental scope, aiming to accommodate a wider array of temperature differentials.

## 6 CONCLUSIONS

This study addresses existing gaps by conducting TE material characterization, comparing three prevalent formulae using vendor datasheets, designing a laboratory test facility for model validation and refinement, and summarize the recommended data extraction procedures. The detailed conclusions are as follows:

- Properties of the bismuth telluride family materials are reviewed in this paper, revealing differences of up to 39.3%, 76.8%, and 57.0% for  $s$ ,  $\rho$ , and  $\kappa$ , depending on the material and doping percentage; thus, extracting properties from the literature without detailed material information is not advisable.
- In the near-room temperature range,  $s$  exhibits a maximum variation of 4.5%, while  $\rho$  and  $\kappa$  change up to 25% and 9%, respectively; as such, properties  $R$  and  $K$  are functions of temperature and not constants.
- Weera's and Luo's methods closely align with the vendor's datasheet data for cooling capacity and voltage, exhibiting an error margin of only 0.1%. These methods are recommended for scenarios with a fixed  $T_h$  and variable  $T_c$ . Conversely, Chen and Snyder's method is not advisable for use under these specific conditions.
- The limitation of Weera's and Luo's approaches, which require a very small temperature lift, is emphasized in this paper; based on the authors' experiments, a 15-K threshold is recommended.
- A test facility was developed, and the results show that  $S$ ,  $R$ , and  $K$  values changed by 0.3%, 6%, and 5%, respectively, when the temperature changed by 15 K. These differences will result in 0.4%, 6%, and 4% variations in cooling capacity calculations.
- Experimental results reveal that, except for  $K$ , the  $S$  and  $R$  values significantly deviated from the vendor's data, causing the performance ( $ZT$ ) to be only half of the vendor's report. Variations in the properties can result in a 40% discrepancy in cooling capacity estimation.

For future work, a new test facility will to be developed to assess TE material properties over a wider temperature range (-20 ~ 100 °C).

## AUTHORSHIP CONTRIBUTION STATEMENT

**Hanlong Wan:** Conceptualization, Methodology, Validation, Formal analysis, Software, Writing - Original Draft, Visualization, Investigation. **Bo Shen:** Supervision, Funding acquisition, Project administration. **Zhenning Li:** Supervision, Methodology, Writing - Review & Editing.

## DECLARATION OF COMPETING INTEREST

The authors declare that they have no known competing financial interests or personal relationships that could have appeared to influence the work reported in this paper.

### **ACKNOWLEDGMENTS**

This work was sponsored by the US Department of Energy's (DOE's) Building Technologies Office under Contract No. DE-AC05-00OR22725 with UT-Battelle LLC. This research used resources at the Building Technologies Research and Integration Center, a DOE Office of Science User Facility operated by the Oak Ridge National Laboratory. The authors would also like to acknowledge Tony Bouza, Technology Manager – HVAC&R, Water Heating, and Appliance, DOE Building Technologies Office.

## REFERENCES

- [1] Dresselhaus MS, Chen G, Tang MY, Yang RG, Lee H, Wang DZ, et al. New directions for low-dimensional thermoelectric materials. *Advanced Materials* 2007;19:1043–53.
- [2] Lv S, Qian Z, Hu D, Li X, He W. A comprehensive review of strategies and approaches for enhancing the performance of thermoelectric module. *Energies* 2020;13:3142.
- [3] Riffat SB, Ma X, Wilson R. Performance simulation and experimental testing of a novel thermoelectric heat pump system. *Applied Thermal Engineering* 2006;26:494–501. <https://doi.org/10.1016/j.applthermaleng.2005.07.016>.
- [4] Chang Y-W, Chang C-C, Ke M-T, Chen S-L. Thermoelectric air-cooling module for electronic devices. *Applied Thermal Engineering* 2009;29:2731–7.
- [5] Zhang HY. A general approach in evaluating and optimizing thermoelectric coolers. *International Journal of Refrigeration* 2010;33:1187–96.
- [6] Zhu L, Tan H, Yu J. Analysis on optimal heat exchanger size of thermoelectric cooler for electronic cooling applications. *Energy Conversion and Management* 2013;76:685–90.
- [7] Liang K, Li Z, Chen M, Jiang H. Comparisons between heat pipe, thermoelectric system, and vapour compression refrigeration system for electronics cooling. *Applied Thermal Engineering* 2019;146:260–7. <https://doi.org/10.1016/j.applthermaleng.2018.09.120>.
- [8] Bansal PK, Martin A. Comparative study of vapour compression, thermoelectric and absorption refrigerators. *International Journal of Energy Research* 2000;24:93–107. [https://doi.org/10.1002/\(SICI\)1099-114X\(200002\)24:2<93::AID-ER563>3.0.CO;2-6](https://doi.org/10.1002/(SICI)1099-114X(200002)24:2<93::AID-ER563>3.0.CO;2-6).
- [9] Çağlar A. Optimization of operational conditions for a thermoelectric refrigerator and its performance analysis at optimum conditions. *International Journal of Refrigeration* 2018;96:70–7. <https://doi.org/10.1016/j.ijrefrig.2018.09.014>.
- [10] Abderezzak B, Dreepaul RK, Busawon K, Chabane D. Experimental characterization of a novel configuration of thermoelectric refrigerator with integrated finned heat pipes. *International Journal of Refrigeration* 2021;131:157–67. <https://doi.org/10.1016/j.ijrefrig.2021.05.013>.
- [11] Duan L, Han J, Cao L, Huo C. Experimental study on heat transfer characteristics of CNTs/Al<sub>2</sub>O<sub>3</sub>nanofluids in personal cooling system based on thermoelectric refrigeration. *Procedia Engineering* 2017;205:588–95. <https://doi.org/10.1016/j.proeng.2017.10.421>.
- [12] Kumar N, Gluesenkamp KR, Rendall J, Patel V, Gehl T, Abu-Heiba A, et al. Experimental Results for Novel Dishwasher with Thermal Storage and Thermoelectric Heat Recovery 2021.
- [13] Patel VK, Gluesenkamp KR, Goodman D, Gehl A. Experimental evaluation and thermodynamic system modeling of thermoelectric heat pump clothes dryer. *Applied Energy* 2018;217:221–32. <https://doi.org/10.1016/j.apenergy.2018.02.055>.
- [14] Patel V, Gluesenkamp KR. Thermoelectric Heat Pump Clothes Dryer using Secondary Loop Heat Exchangers: Experimental Evaluation and System Modeling, 2018.
- [15] Goldsmid H. Thermoelectric Refrigeration. Springer; 2013.
- [16] Titov OY, Bulat LP, Gurevich YG. Nature of the thermoelectric power in bipolar semiconductors. *International Journal of Thermophysics* 2016;37:1–13.
- [17] Gurevich YG, VELAZQUEZ-PEREZ JE. Peltier effect in semiconductors. *Wiley Encyclopedia of Electrical and Electronics Engineering* 1999:1–21.
- [18] Zhao D, Tan G. A review of thermoelectric cooling: Materials, modeling and applications. *Applied Thermal Engineering* 2014;66:15–24. <https://doi.org/10.1016/j.applthermaleng.2014.01.074>.
- [19] Luo Z. A simple method to estimate the physical characteristics of a thermoelectric cooler from vendor datasheets. *Electronics Cooling* 2008;14:22–7.
- [20] Hsu C-T, Huang G-Y, Chu H-S, Yu B, Yao D-J. An effective Seebeck coefficient obtained by experimental results of a thermoelectric generator module. *Applied Energy* 2011;88:5173–9. <https://doi.org/10.1016/j.apenergy.2011.07.033>.

- [21] Chen M, Snyder GJ. Analytical and numerical parameter extraction for compact modeling of thermoelectric coolers. *International Journal of Heat and Mass Transfer* 2013;60:689–99. <https://doi.org/10.1016/j.ijheatmasstransfer.2013.01.020>.
- [22] Witting IT, Chasapis TC, Ricci F, Peters M, Heinz NA, Hautier G, et al. The Thermoelectric Properties of Bismuth Telluride. *Advanced Electronic Materials* 2019;5:1800904. <https://doi.org/10.1002/aelm.201800904>.
- [23] Cho H, Back SY, Yun JH, Byeon S, Jin H, Rhyee J-S. Thermoelectric Properties and Low-Energy Carrier Filtering by Mo Microparticle Dispersion in an n-Type  $(\text{CuI})_{0.003}\text{Bi}_2(\text{Te,Se})_3$  Bulk Matrix. *ACS Appl Mater Interfaces* 2020;12:38076–84. <https://doi.org/10.1021/acsami.0c09529>.
- [24] Kim G, Lee K, Shin H, Kim J, Chang J, Roh JW, et al. Strong enhancement of room-temperature thermoelectric properties of Cu-doped  $\text{Bi}_2\text{Te}_{2.7}\text{Se}_{0.3}$ . *Appl Phys Lett* 2022;120:043903. <https://doi.org/10.1063/5.0077057>.
- [25] Tiadi M, Satapathy DK, Battabyal M. Evolution of optical phonon modes and thermoelectric properties in doped  $\text{Bi}_2\text{Te}_3$ : A temperature-dependent Raman spectroscopy study. *Phys Rev Materials* 2023;7:015401. <https://doi.org/10.1103/PhysRevMaterials.7.015401>.
- [26] Cai Y, Wang Y, Liu D, Zhao F-Y. Thermoelectric cooling technology applied in the field of electronic devices: Updated review on the parametric investigations and model developments. *Applied Thermal Engineering* 2019;148:238–55.
- [27] Lineykin S, Ben-Yaakov S. Analysis of thermoelectric coolers by a spice-compatible equivalent-circuit model. *IEEE Power Electronics Letters* 2005;3:63–6.
- [28] Weera S, Lee H, Attar A. Utilizing effective material properties to validate the performance of thermoelectric cooler and generator modules. *Energy Conversion and Management* 2020;205:112427. <https://doi.org/10.1016/j.enconman.2019.112427>.
- [29] Yin T, He Z-Z. Analytical model-based optimization of the thermoelectric cooler with temperature-dependent materials under different operating conditions. *Applied Energy* 2021;299:117340. <https://doi.org/10.1016/j.apenergy.2021.117340>.
- [30] Patel VK, Gluesenkamp KR, Boudreaux P. Thermoelectric heat pump performance characterization. 13th IEA Heat Pump Conference 2021 Conference Proceedings, Jeju, South Korea: 2021, p. 1166 to 1172.
- [31] Attar A, Lee H, Snyder GJ. Optimum load resistance for a thermoelectric generator system. *Energy Conversion and Management* 2020;226:113490. <https://doi.org/10.1016/j.enconman.2020.113490>.
- [32] Siddique ARM, Venkateshwar K, Mahmud S, Van Heyst B. Performance analysis of bismuth-antimony-telluride-selenium alloy-based trapezoidal-shaped thermoelectric pallet for a cooling application. *Energy Conversion and Management* 2020;222:113245. <https://doi.org/10.1016/j.enconman.2020.113245>.
- [33] Mohammadpour M, Houshfar E, Ashjaee M. Performance evaluation and multi-objective optimization of an innovative solar-assisted multigeneration energy storage system for freshwater/O<sub>2</sub>/H<sub>2</sub> generation. *Sustainable Energy Technologies and Assessments* 2022;53:102755. <https://doi.org/10.1016/j.seta.2022.102755>.
- [34] Buchalik R, Nowak G, Nowak I. Mathematical model of a thermoelectric system based on steady- and rapid-state measurements. *Applied Energy* 2021;293:116943. <https://doi.org/10.1016/j.apenergy.2021.116943>.
- [35] Alomair Y, Alomair M, Mahmud S, Abdullah HA. Theoretical and experimental analyses of solar-thermoelectric liquid-chiller system. *International Journal of Refrigeration* 2015;56:126–39.
- [36] Zhao D, Lu X, Fan T, Wu YS, Lou L, Wang Q, et al. Personal thermal management using portable thermoelectrics for potential building energy saving. *Applied Energy* 2018;218:282–91.
- [37] Zhao D, Tan G. Experimental evaluation of a prototype thermoelectric system integrated with PCM (phase change material) for space cooling. *Energy* 2014;68:658–66. <https://doi.org/10.1016/j.energy.2014.01.090>.
- [38] Byon Y-S, Jeong J-W. Annual energy harvesting performance of a phase change material-integrated thermoelectric power generation block in building walls. *Energy and Buildings* 2020;228:110470.

- [39] Khire RA, Messac A, Van Dessel S. Design of thermoelectric heat pump unit for active building envelope systems. *International Journal of Heat and Mass Transfer* 2005;48:4028–40.
- [40] Wan H, Gluesenkamp KR, Shen B, Li Z, Patel VK, Kumar N. A Thermodynamic Model of Integrated Liquid-to-Liquid Thermoelectric Heat Pump Systems. *International Journal of Refrigeration* 2023.
- [41] Winterton RH. Where did the Dittus and Boelter equation come from? *International Journal of Heat and Mass Transfer* 1998;41:809–10.
- [42] Huang B-J, Chin CJ, Duang CL. A design method of thermoelectric cooler. *International Journal of Refrigeration* 2000;23:208–18.
- [43] Fraisse G, Ramousse J, Sgorlon D, Goupil C. Comparison of different modeling approaches for thermoelectric elements. *Energy Conversion and Management* 2013;65:351–6.

## Appendix

### Appendix 1 – Materials properties literature review (original data)

See attached database.

### Appendix 2 – Experimental row data (reported in the paper)

Number	Thotin [°C]	Thoutou t [°C]	Tcoldin [°C]	Tcoldou t [°C]	Tcoldsur fin [°C]	Tcoldsur fout [°C]	Thotsurf in [°C]	Thotsurf out [°C]	U [V]	MFR [kg/s]
1	20.35	21.11	19.29	18.81	18.42	16.70	21.28	27.08	26.58	0.04
2	24.92	25.44	21.04	20.71	19.71	18.98	25.83	30.16	27.73	0.06
3	27.13	27.63	20.17	19.88	18.95	18.30	27.90	32.05	28.50	0.06
4	26.79	27.48	19.02	18.62	18.29	16.91	27.35	32.64	28.27	0.04
5	25.54	26.69	20.06	19.46	18.77	15.44	26.80	34.77	29.36	0.02
6	29.67	30.17	20.06	19.80	18.96	18.39	30.29	34.42	29.15	0.06
7	25.73	26.88	20.04	19.43	18.76	15.44	26.97	34.96	29.41	0.02
8	26.25	27.41	20.01	19.42	18.76	15.50	27.47	35.42	29.52	0.02
9	27.00	28.16	19.99	19.42	18.77	15.55	28.20	36.10	29.69	0.02
10	31.18	31.81	19.04	18.69	18.40	17.26	31.53	36.57	29.35	0.04
11	28.45	29.61	19.97	19.42	18.80	15.76	29.58	37.47	30.00	0.02
12	30.66	31.83	19.94	19.43	18.87	16.05	31.67	39.36	30.55	0.02
13	34.51	35.12	19.13	18.82	18.56	17.62	34.70	39.65	30.21	0.04
14	35.69	36.30	19.19	18.89	18.63	17.78	35.83	40.76	30.51	0.04
15	36.30	36.90	19.29	18.98	18.74	17.92	36.43	41.33	30.65	0.04
16	36.94	37.54	19.49	19.19	18.95	18.15	37.05	41.93	30.78	0.04
17	34.20	35.32	19.92	19.48	18.97	16.51	35.04	42.33	31.35	0.02
18	37.44	38.04	19.96	19.64	19.39	18.66	37.56	42.43	30.85	0.04
19	37.36	37.97	19.81	19.50	19.27	18.51	37.47	42.34	30.86	0.04
20	37.54	38.58	19.92	19.52	19.08	16.93	38.21	45.08	32.08	0.02
21	39.22	40.19	19.93	19.56	19.15	17.14	39.80	46.40	32.49	0.02
22	42.12	42.50	19.80	19.62	19.17	18.90	42.20	46.19	32.44	0.06
23	39.94	40.86	19.93	19.56	19.17	17.23	40.48	46.89	32.63	0.02
24	40.66	41.58	20.20	19.82	19.41	17.45	41.17	47.50	32.77	0.02

### Appendix 3 – VT-199-1.4-0.8 Test Results

#### 1) Seebeck voltage measurements

Temperature lift [K]	Seebeck Voltage [V]
4.35	1.08
5.74	1.42
7.13	1.71
8.31	2.00
9.31	2.27

10.27	2.52
11.03	2.74
11.86	2.97
12.62	3.14
13.25	3.29
13.81	3.43
14.27	3.57
14.65	3.69
15.07	3.79
15.43	3.88
15.79	3.97
16.00	4.01
16.22	4.09
16.41	4.13
16.60	4.18
16.72	4.21
16.81	4.24
16.92	4.27
17.02	4.28
17.11	4.33
17.20	4.35
17.32	4.36
17.36	4.40
17.45	4.42
17.53	4.43
17.57	4.44

2) Heat transfer

Voltage [V]	Current [A]	DT [K]	Seebeck Voltage [V]	MFR [kg/s]	Hot side capacity [W]	Cold side capacity [W]	Energy balance [W]	[%]	Heating COP [-]	Cooling COP [-]
22.08	2	4.345	1.08	0.04	125.42	98.08	14.67	33.21%	2.84	2.22
22.47	2	5.74	1.42	0.04	120.59	91.65	13.16	29.28%	2.68	2.04
22.82	2	7.13	1.71	0.04	117.38	85.22	10.06	22.05%	2.57	1.87
23.17	2	8.305	2	0.04	112.55	82	11.79	25.44%	2.43	1.77
23.45	2	9.305	2.27	0.04	107.73	77.18	11.81	25.18%	2.3	1.65
23.76	2	10.265	2.52	0.04	104.51	73.96	11.93	25.10%	2.2	1.56
24.06	2	11.025	2.74	0.04	101.3	70.75	12.09	25.12%	2.11	1.47
24.27	2	11.86	2.97	0.04	99.69	67.53	10.44	21.51%	2.05	1.39
24.51	2	12.62	3.14	0.04	96.47	64.32	10.58	21.59%	1.97	1.31
24.39	2	13.25	3.29	0.04	94.87	62.71	10.04	20.59%	1.94	1.29
24.87	2	13.81	3.43	0.04	90.04	57.88	10.72	21.56%	1.81	1.16
25.04	2	14.265	3.57	0.04	91.65	57.88	9.17	18.32%	1.83	1.16

25.17	2	14.645	3.69	0.04	90.04	56.28	9.19	18.26%	1.79	1.12
25.29	2	15.065	3.79	0.04	88.44	54.67	9.23	18.26%	1.75	1.08
25.41	2	15.425	3.88	0.04	86.83	53.06	9.29	18.29%	1.71	1.04
25.51	2	15.785	3.97	0.04	85.22	51.45	9.31	18.26%	1.67	1.01
25.58	2	16	4.01	0.04	85.22	49.85	7.77	15.18%	1.67	0.97
25.65	2	16.22	4.09	0.04	85.22	49.85	7.75	15.10%	1.66	0.97
25.72	2	16.41	4.13	0.04	83.61	48.24	7.81	15.17%	1.63	0.94
25.79	2	16.595	4.18	0.04	83.61	49.85	9.45	18.33%	1.62	0.97
25.83	2	16.72	4.21	0.04	82	49.85	11.08	21.45%	1.59	0.96
25.86	2	16.81	4.24	0.04	83.61	48.24	7.87	15.21%	1.62	0.93
25.9	2	16.92	4.27	0.04	82	46.63	7.89	15.22%	1.58	0.9
25.93	2	17.015	4.28	0.04	82	48.24	9.53	18.38%	1.58	0.93
25.96	2	17.11	4.33	0.04	80.4	48.24	11.1	21.38%	1.55	0.93
25.97	2	17.195	4.35	0.04	80.4	49.85	12.69	24.43%	1.55	0.96
26.02	2	17.315	4.36	0.04	82	48.24	9.55	18.36%	1.58	0.93
26.05	2	17.36	4.4	0.04	80.4	48.24	11.14	21.39%	1.54	0.93
26.07	2	17.445	4.42	0.04	78.79	48.24	12.75	24.45%	1.51	0.93
26.11	2	17.53	4.43	0.04	80.4	48.24	11.2	21.45%	1.54	0.92
26.12	2	17.565	4.44	0.04	80.4	46.63	9.59	18.36%	1.54	0.89

#### Appendix 4 – Vendors’ datasheet

	inbTC1-127.06		VT-199-1.4-0.8	
$T_h$	27	50	27	50
$\Delta T_{max}$	74	83	69	78
$U_{max}$	16.8	18.08	24.6	27.3
$I_{max}$	6.3	6.3	11.3	11.3
$Q_{max}$	66	73.6	172	188.7